Thomas Siegmund
School of Mechanical Engineering,
Purdue University,
West Lafayette, IN 47907
e-mail: siegmund@purdue.edu

Francois Barthelat
Department of Mechanical Engineering,
McGill University,
Montreal, QC H3A 2K6, Canada
e-mail: francois.barthelat@mcgill.ca

Raymond Cipra
School of Mechanical Engineering,
Purdue University,
West Lafayette, IN 47907
e-mail: cipra@purdue.edu

Ed Habtour
Vehicle Technology Directorate,
RDRL-VTM,
U.S. Army Research Laboratory,
Aberdeen Proving Ground, MD 21005

Jaret Riddick
Vehicle Technology Directorate,
RDRL-VTM,
U.S. Army Research Laboratory,
Aberdeen Proving Ground, MD 21005

Manufacture and Mechanics of Topologically Interlocked Material Assemblies

Topologically interlocked material (TIM) systems are load-carrying assemblies of unit elements interacting by contact and friction. TIM assemblies have emerged as a class of architectured materials with mechanical properties not ordinarily found in monolithic solids. These properties include, but are not limited to, high damage tolerance, damage confinement, adaptability, and multifunctionality. The review paper provides an overview of recent research findings on TIM manufacturing and TIM mechanics. We review several manufacturing approaches. Assembly manufacturing processes employ the concept of scaffold as a unifying theme. Scaffolds are understood as auxiliary support structures employed in the manufacturing of TIM systems. It is demonstrated that the scaffold can take multiple forms. Alternatively, processes of segmentation are discussed and demonstrated. The review on mechanical property characteristics links the manufacturing approaches to several relevant material configurations and details recent findings on quasi-static and impact loading, and on multifunctional response. [DOI: 10.1115/1.4033967]

1 Introduction

Architectured materials are considered as alternatives to conventional materials and have been proposed as solutions to fill expand the available material property spaces [1–4]. This emerging class of materials is characterized by specific and periodic structural features which are larger than what is typically considered a microstructural length scale (such as a grain size) but smaller than the size of the final component made of the architectured material. This class of materials includes, but is not limited to, lattice materials and cellular material systems [5,6], periodically patterned thin-walled materials [3,7], periodic granular crystals in 2D and 3D [8,9], as well as dense material systems composed of building blocks of well-defined size and shape [1]. These principles can be applied individually, in combination, or in a nested approach. In architectured materials, there exist multiple strategies to improve the component performance. In architectured material, component properties can emerge solely from the material architecture and the imposed specific geometric pattern without changing the materials properties [3,5,7,9] (shape in the notation of Ref. [1]). Yet, architectured materials also provide a pathway to embed size-dependent material properties (shape and scale [1]). Ultralow density metallic cellular solids exploit a size effect of plasticity to extend the regime of elastic deformation response [10]. Segmented material systems allow to exploit size effects related to brittle fracture, either stemming from statistical aspects [1] or from fracture length scale considerations [11]. Finally, architectured materials can be multiphase (shape, scale, and composite [1]). Sandwich structures with one material as a facesheet and a second in the core are one such example [12].

Here, we are concerned with architectured material systems based on the principle of assembly and/or segmentation. Thereby, the architecture material is made by either a bottom-up process of the ordered assembly of unit elements or top-down by the segmentation of an existing monolithic solid. Individual unit elements mechanically interact with each other by contact and friction. No form adhesive bonding between unit elements is in place. Rather, the overall assembly is held together by either internal or external constraints such that a load-carrying architectured material is obtained. Cable systems can be considered as 1D architectured material either made by segmentation of a monolithic beam–truss system or alternatively as a 1D assembly of a plurality of 1D elements—wires. The 1D architectured material possesses high stiffness in the axial direction by a much higher bending flexibility than the monolithic equivalent. Unbonded laminates (e.g., a laminate spring) can be considered as a 2D architectured material either made by a layered segmentation of a monolithic plate or alternatively as an assembly of 2D elements—plates. The 2D architecture possesses high in-plane stiffness and higher bending flexibility than the monolithic equivalent. A planar puzzle is an alternate 2D architectured material either made by through-thickness segmentation of a monolithic plate or alternatively as an assembly of 2D elements as interconnected puzzle pieces [1,13]. The 2D architecture possesses high in-plane stiffness and combined with high damage tolerance. Such a planar puzzle possesses favorable failure statistics [1]. Architecture constructs based on the assembly of discrete unit blocks have both a long tradition [14] and current developments [15–17]. There exists a substantial array of work in the domain of masonry engineering where a wide range of different unit element shapes have been considered. In these *stereotomic structures*, the discrete pieces are held together primarily by their own gravitational force, and the external loads are considered only in the context of the main gravitational load. These systems have not been the focus of the present review.

The present review article focusses on a class of architectured materials that emerge from segmenting space (or filling space) by periodic arrangements of identical polyhedra on periodic lattices. This problem itself is of classical relevance in mathematics. Then,

Manuscript received March 9, 2016; final manuscript received May 17, 2016; published online July 14, 2016. Editor: Harry Dankowicz.

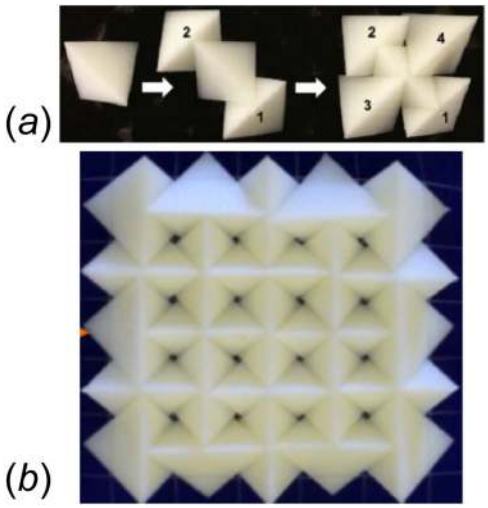

Fig. 1 Example of a TIM system: (*a*) a plurality of unit elements and the principle of topological interlocking. (Reproduced with permission from Khandelwal et al. [35]. Copyright 2015 by IOP Publishing Limited.) (*b*) A topologically interlocked architectured material.

a load-carrying architectured material is achieved if the geometry of the individual unit element enables topological confinement by the adjacent unit elements. The resulting architectured materials are called TIM systems.

Figure 1 depicts one possible configuration of a TIM system. This particular configuration represents a 2D architectured material. The TIM system is obtained by initially considering individual unit elements of polyhedra shape (tetrahedra in the present case). These tetrahedra are arranged on a square lattice. Then, adjacent tetrahedra have two parallel faces. Since the adjacent tetrahedra are rotated 90 deg to each other, the relative rigid body motion is constraint. The particular configuration shown is that of a dense packing of tetrahedra in a plane [18]. Other geometric configurations for the unit elements and the respective assemblies have been considered. Key rules for the construction of such architectured materials have been established for 2D regular lattices [19] and were recently extended to semiregular lattices [20]. With an origin in structural mechanics (Abeille's dome as reviewed in Ref. [21]), a modern version of a topologically interlocked architectured material was proposed by Glickman [22] in the context of paving system. Subsequently, the interlocking concept was proposed in the context of engineering applications [23], and the term TIM systems was introduced [24,25]. No limitations exist, in theory, on which material class can be used. TIMs can be made of metallic [26], ceramic [13,27], polymeric [26,28], unit elements, or even of ice [29]. Heterogeneous TIMs can combine material elements from each class. Finally, there exist a range of possible approaches on how to provide the constraint to the TIM system including rigid external or flexible external system boundaries, internal or external tension cables, as well as self-supported assemblies [30].

TIM system was found to possess interesting and unusual mechanical properties. A negative elastic stiffness of TIMs was documented [26,31,32] and also reproduced in computer simulations. These studies attribute this finding to a change in the contact conditions from face-to-face to face-to-vertex configuration during loading and the reversal of this process during unloading. Several investigations demonstrated high damage tolerance for TIMs under quasi-static loading as cracks are arrested at unit-to-unit contact surfaces [24]. This feature enables one to construct architectured materials in which brittle solids are transformed into architectured materials with high damage tolerance through the architecture of the material [13]. The damage confinement due to crack arrest at the contact surfaces enables that TIMs can be readily remanufactured after complete failure without a significant loss of properties [33]. In Ref. [11], it was demonstrated that the enhanced damage tolerance inherent to TIMs can be realized also for certain ranges of dynamic loading conditions. Recently, Estrin and coworkers [34] demonstrated the control of TIM system stiffness through active control of the internal constraint, while Khandelwal et al. [35] showed the adaptive characteristics of TIMs to energy absorption based on control of the external constraint. Carlesso et al. [36,37] illustrated that TIM systems can possess enhanced sound absorption, based on the dynamic contact processes among basic building blocks.

This paper is structures as follows. In Sec. 2, several manufacturing methods for TIMs are reviewed. Bréchet [38] conceptually suggests several manufacturing approaches, but no specific examples are given. The present paper aims to fill this gap and reports details on several relevant approaches for manufacturing of TIMs. These are grouped into bottom-up methods (assembly methods and 3D printing) and top-down methods (segmentation). The commonality among all manufacturing approaches discussed here is the presence of a scaffold. Scaffolds are understood as auxiliary support systems enabling the assembly of structures from unit elements. While in the construction of stereotomic structures (arches and domes) and also for TIM-type civil engineering solutions rigid scaffolds are common, for advanced materials engineering applications the concept of the scaffold is re-examined and the scope of the scaffold is expanded. In Sec. 3, experimental evidence of mechanical properties and the mechanics of TIMs are reviewed. The paper concludes with a summary and outlook.

2 Methods of Manufacture for TIMs

2.1 Assembly. The discrete nature of TIM systems requires the use of some form of scaffold during manufacturing. The use of such scaffolds is common in the construction of arches and dome structures where self-weight is a central feature. For the engineering TIM systems of interest here, the topological interlocking geometry introduces additional constraints. On the other hand, there is no need to restrict considerations to the rigid scaffolds of civil engineering. For manufacturing of TIMs by assembly, the starting point is a plurality of (polyhedra) unit elements. Such unit elements can be produced by a range of methods, including conventional computer numerical control (CNC) machining, casting [27], or additive manufacturing [28].

2.1.1 Directional Pick and Place. Pick-and-place assembly processes use machine tools to place individual parts on predefined locations. Commonly, the individual parts are moved along the direction orthogonal to the assembly plane, and individual parts are not in contact with each other. For TIM systems assemblies, this basic pick-and-place approach is not possible as the interlocking geometry of the unit elements and the specific periodicity of the assembly (Fig. 1) introduces two additional constraints. To account for these constraints, a pick-and-place process for TIMs needs to consider directionality of both the unit elements in the assembly plane and the positioning approach, and embed both steps into the assembly sequence.

For TIM assembly, unit elements need not be placed only in the assembly plane, but subsequent directed motion in the assembly plane is necessary to achieve the topological interlocking geometry. Furthermore, unit elements need to be positioned in specific orientation. As an example, for the assembly of Fig. 1, tetrahedra are positioned with two edges aligned with the assembly plane. These two edges are orthogonal to each other. Based on these two geometric features, the assembly approach requires that 0 deg and 90 deg oriented tetrahedra, respectively, are moved along one of the assembly plane in alternate sequence (Fig. 2). In the assembly process depicted in Fig. 2, gravity provides the directionality for the assembly. A U-shaped *rigid scaffold* provides the constraint during assembly. The frame is made of pieces possessing prismatic shape such that their cross section engages with the sides of the TIM assembly. Tetrahedra are positioned in the drop plane

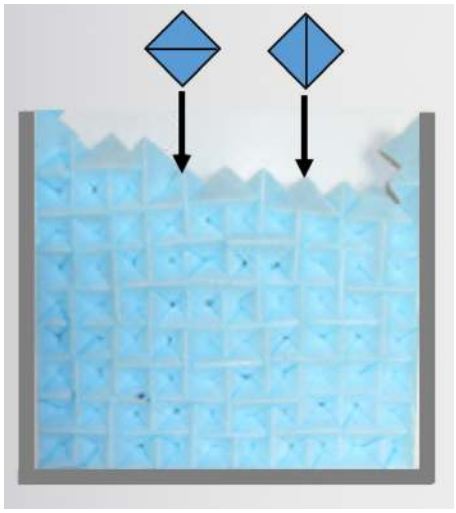

Fig. 2 TIM assembly with gravity assist in a U-shaped rigid scaffold. Individual unit elements are made of a rigid polymer foam and shaped by a wire cutting process [39]. Unit elements edge length of $a = 25.0$ mm.

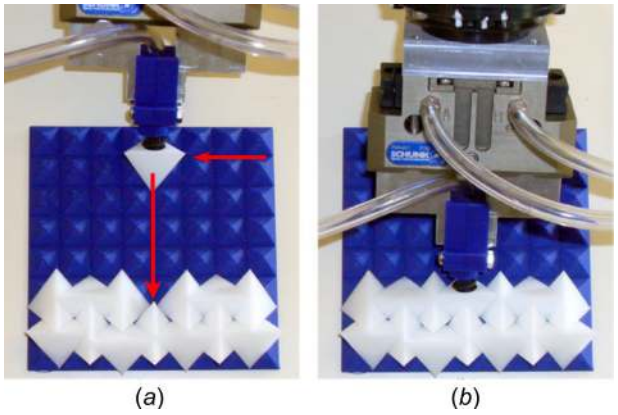

Fig. 3 Assembly with rigid scaffold plane and a template. Individual unit elements made by fused deposition 3D printing, unit elements edge length of $a = 25.0$ mm. (Reproduced with permission from Mather et al. [33]. Copyright 2012 by Emerald Group Publishing Limited.)

and placed in a sequence of alternating 0 deg and 90 deg. Once the desired assembly is completed, the fourth edge of the frame is put in place to constrain the assembly and a complete TIM system is obtained. This approach has been documented as successful for the assembly of TIM systems for civil engineering applications, i.e., the construction of a TIM wall for a building structure [40].

Instead of using gravity, a *rigid scaffold plane with an inscribed template* can be used to provide directionality. Then, the assembly plane is not constrained to the direction perpendicular to ground. Figure 3 depicts the assembly on such a scaffold. The assembly process of a TIM based on $n \times n$ tetrahedra units is enabled by a scaffold consisting of $n \times n$ square pyramids which are positioned on a square grid. The edge of each of the square pyramids equals half of the tetrahedra edge length. In the embodiment of the process shown in Fig. 3, a robotic system equipped with a vacuum gripping system was used to pick up unit elements from a source, transport these to the assembly scaffold, and place them with alternating 0 deg and 90 deg orientation. The template provides two orthogonal assembly motions for the tetrahedra which need to be moved sequentially in alternating assembly directions corresponding to their 0 deg and 90 deg orientation relative to the scaffold. There exist TIM configurations, e.g., osteomorphic bricks [41] and truncated tetrahedra, where the support against tipping of the unit elements is not required and assembly can be performed on a flat scaffold but the principles of directionality embedded in the template remain in place for these cases as well. TIM systems are not restricted to be planar. If the geometry of the unit element is appropriately distorted, complex TIM shapes can be achieved. In such cases, the scaffold is not restricted to be planar [16]. When considering robotic TIM assembly processes, speeds and scales are defined by the capabilities of the robotic devices employed, with typical assembly rates of 100–1000 unit elements per minute. Once the assembly is complete, the TIM system can be confined externally and be lifted off the template (Fig. 4(*a*)). Alternatively, the scaffold can become a functional part of the TIM system. In Ref. [12], the authors report on a sandwich panel with a core made of a TIM system based on osteomorphic brick (Fig. 4(*b*)). In such a hybrid TIM system, the scaffold then becomes one of the facesheets.

2.1.2 Parallel Assembly. Both directional pick-and-place methods require not only the exact positioning of individual unit elements but also the directed motion of unit elements along specific paths defined for each specific unit element. These limitations can be removed if a *deformable scaffold* is considered, see Fig. 5 for a schematic drawing and Fig. 6 for physical system realization. The deformable scaffold is constructed from two sets of orthogonal strings forming an orthogonal template with initial grid spacing w. The grid is subsequently collapsed into a grid with spacing w'. Unit elements are placed on the scaffold following the template pattern in the *open* state of the scaffold, and subsequently, interlocking is achieved simultaneously for all unit elements of the TIM assembly by differential scaling of the scaffold grid to its *closed* state, Figs. 5(*b*) and 6(*c*), respectively.

The underpinning concept of the parallel assembly is that a robot would perform a basic pick-and-place operation onto a rectangular template in which no interlocking of unit elements is yet

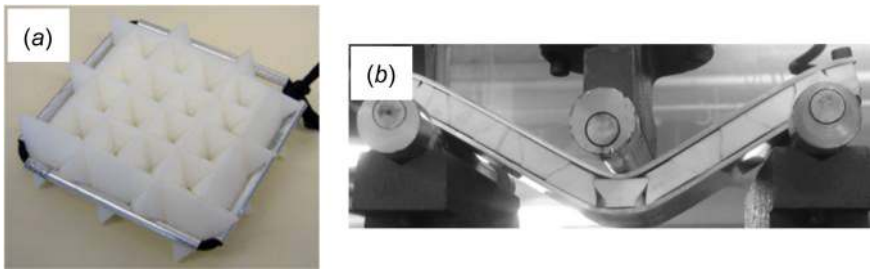

Fig. 4 (*a*) TIM system removed from the scaffold and externally constrained. In this configuration, the external constraint is provided by a prestressed elastic cable guided in tubes. (*b*) A sandwich panel with a TIM core. In this hybrid TIM system, the scaffold becomes the sandwich facesheet. (Reproduced with permission from Molotnikov et al. [12]. Copyright 2013 by WILEY-VCH Verlag.)

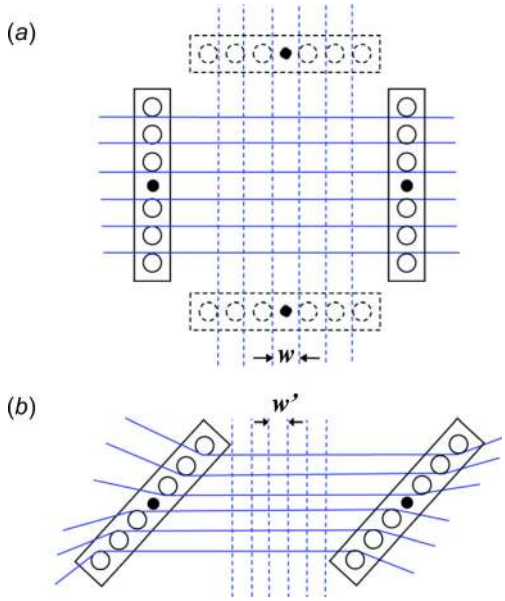

Fig. 5 Deformable (string) scaffold in (*a*) the *open* state with grid spacing *w* and (*b*) the *closed* state with grid spacing *w′*, achieved by differential scaling of the scaffold grid [39].

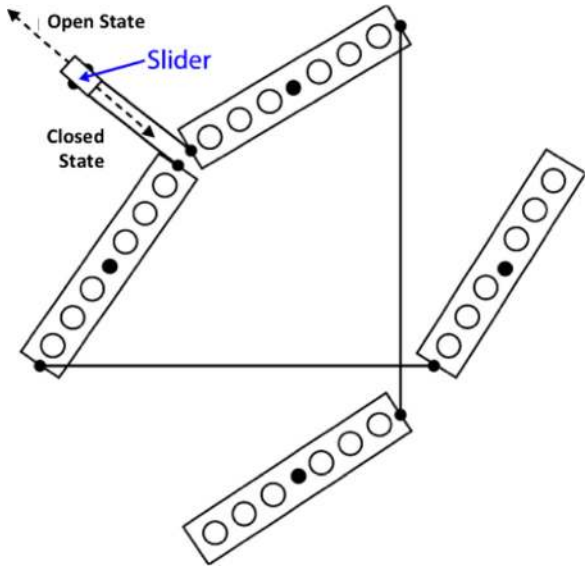

Fig. 7 Mechanism overview for the deformable string scaffold [39].

present (Fig. 6(*a*)). In the *open* configuration of the scaffold, individual unit elements are placed without the need for exact positioning (Fig. 6(*b*)). In the *closed* state of the scaffold, individual unit elements are then in the position required for the topologically interlocked assembly overall (Fig. 5(*c*)). The scaffold is embodied by two orthogonally positioned groups of strings, and a mechanism enables that this scaffold of strings only goes through a differential scaling, with rotation, skew, and translation excluded.

Considering the tetrahedra edge length a, the grid spacing w is at least $\sin(45\,\text{deg})a$ but less than a. Experience showed that a value of $w = 0.8a$ is practical. The final grid spacing is w'. Furthermore, the grid must be elevated from ground by distance h for free motion of tetrahedra. Geometry defines $h > (w/2)\tan(54.73\,\text{deg})$. The height position of the grid is ensured by guiding the strings along string guides of at least height h. The selection of the string material and string tension is dependent on the weight of the tetrahedra considered in the assembly. Tension in individual strings was induced by the use of springs attached to the string ends. To enable the differential scaling of the scaffold from grid spacing w to w', parallel rotating string guides are used, a top and bottom set and a left and right set as in Fig. 7. Two coupler links are used with each set of string guides to ensure the parallel rotation between each guide pair (Fig. 6). Each set of string guides is then linked by a coupler (l_2) to a common slider mechanism for actuation of the guides between the open and closed state (Fig. 7). In order to determine the geometry of the slider, a number of geometric constraints must be determined. Geometric quantities are defined in Fig. 8. The length H is the distance between the guide pivot and the line of action of the slider. Following Fig. 8, one obtains $H = l_1\cos(\alpha) + l_2\sin(\theta_{\text{col}})$ as well as $H = l_1\cos(\beta) + l_2\sin(\theta_{\text{exp}})$. The strike of the slider is $s = l_1\sin(\beta) + l_2\cos(\theta_{\text{exp}}) + l_1\sin(\alpha) - l_2\cos(\theta_{\text{col}})$. Hereby, l_1 is the half-length of the string guide link and relates to unit elements in the assembly n and the string spacing w. In the open state, the two sets of strings are perpendicular, so $\beta = 45\,\text{deg}$. To achieve the closed state with the string spacing w', the guide rotation angle $\alpha + \beta$ is required. Once the couple link length l_2 is selected, the system of equations can be solved to obtain the remaining parameters for the mechanisms, stroke s and angles θ_{col}, θ_{exp}. Considering a linear actuator for the slider, a coupler link length was chosen that corresponded to a suitable stroke length for the available linear actuator.

As the assembly process is concluded, the assembly of tetrahedra still contains the strings used for the assembly. These strings can either be seen as sacrificial or be removed once the assembly is placed in its final constraint. Alternatively, the strings introduced by this process can be seen as independent elements which can be used to introduce the constraint not through an external frame but through internal tensile elements. Then, it is of interest to also consider the mechanical properties of the strings. Figure 9 depicts two embodiments of TIMs where carbon fiber tow is used

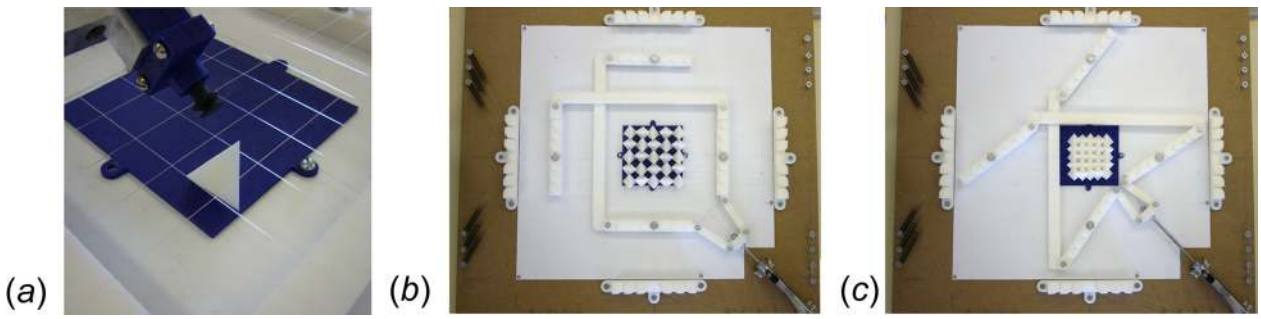

Fig. 6 Mechanism for parallel assembly of a topologically interlocked architectured material with a deformable scaffold: (*a*) initial placement of unit element on grid, (*b*) mechanism in *open* state for the approximate placement of unit elements, and (*c*) mechanism in *closed* state. String guides possess pultrusions to guide the strings individually and are free to rotate about their midspan point [39].

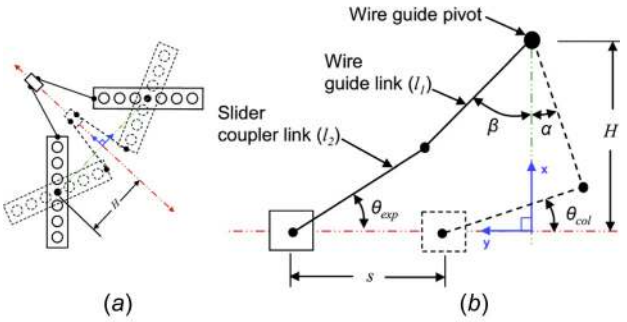

Fig. 8 Mechanism geometry detail: (*a*) positions of wire guides and (*b*) kinematic relationships [39].

to provide the constraint. The two specimens shown were not directly manufactured using the string scaffold, but are used for illustrative purpose. For the two TIM configurations in Fig. 9, the support elements are not continuous and thus by themselves do not provide in-plane constraint. These components only serve to guide the carbon fiber tow and to apply the out-of-plane displacement boundary condition during a loading experiment. There is no principle limitation to which materials are considered as strings, and both passive and active materials can be considered.

2.1.3 Self-Assembly. Self-assembly of millimeter-sized particles has been described in the past [42,43] yet without considering topological interlocking geometries. On the millimeter scales, surface tension and other weak interactions are not strong enough to overcome inertia effects, and stronger interaction forces are required. Magnetic forces are ideal for self-assemble at these large length scales. In addition, mobility needs to be imparted on the unit elements considered for self-assembly. A self-assembly process enabled by a *liquid scaffold* is a relevant approach. Here, we report on a specific self-assembly process where tetrahedra form a dense planar packing at a interface between the liquid and air. In order to enable the self-assembly process of the tetrahedron, each unit now contains four small magnets placed at the centroid position of each tetrahedron facet. Opposing faces are allocated a *plus–plus* or *minus–minus* pairing of poles, respectively, to ensure the directionality of the assembly. Furthermore, the tetrahedra require special consideration for their mobility and orientation in the assembly plane. Floating of tetrahedra is required to be positioned such that one edge is parallel to the bottom of the fluid container. This orientation of the tetrahedron can either accomplished the use of a keel. Classical rules of buoyancy and stability dictate the density of the fluid and the weight of the keel, once a material for the tetrahedra is selected. A typical embodiment of a tetrahedron for such self-assembly process is shown in Fig. 10(*a*). A self-assembled TIM is given in Fig. 10(*b*). After self-assembly, the TIM system can then be placed in a relevant confinement configuration. Magnets can either be left in place or be dissolved. Such a

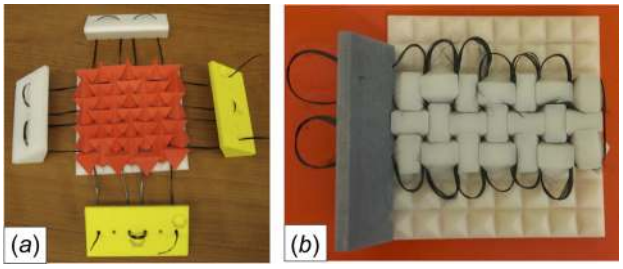

Fig. 9 Two TIM systems with internal constraints: (*a*) a plate-type configuration based on regular tetrahedra [53] and (*b*) a cantilever-type configuration based on truncated tetrahedra. Unit elements are manufactured by fused deposition 3D printing; T300 carbon fiber tow is used as the internal constraint.

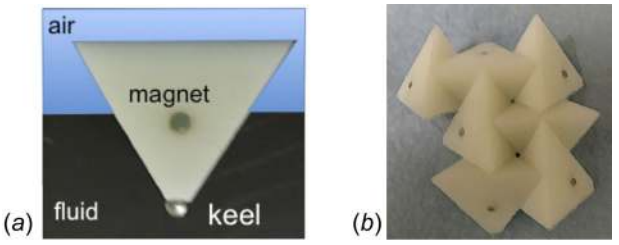

Fig. 10 (*a*) Unit element with features for directional self-assembly at the air–fluid interface. Unit element manufactured by polyjet 3D printing. (*b*) Self-assembled TIM based on unit elements shown.

process can be accomplished with the use of magnets that are based on magnet particle powder embedded in a polymer region.

2.2 Three-Dimensional Printing. Three-dimensional printing approaches allow for the integrated manufacturing of unit cells in the TIM in the final position together with the external constraint. computer-aided design (CAD) software and scripting software are ideal tools to be applied for the creation of the geometric models for the TIM assembly and readily lead to the STereoLithography (STL) files commonly required for 3D print manufacturing. The assembly template is thus readily encoded. A *sacrificial scaffold* is inherent to the print process as a support resin is deposited to enable a multipart 3D print process. Figure 11 shows the printer interface with the CAD model for the TIM with 7×7 tetrahedra and integrated printed system boundary. A key parameter in establishing the model is the definition of a gap between the unit elements such that the units can be released from each other after printing. Such manufacturing-related tolerances are 3D print system dependent. As one example, experience with the Connex 350 printer revealed that a gap size of 0.35 mm allowed for the reliable release of unit elements with $a = 25$ mm. Figure 12(*a*) depicts a final TIM system after removal of the support resin. Metal shim stock along the frame was used to compensate for the printing gap and to control the confinement pressure in the assembly. The additive manufacturing process is ideal suited for the manufacture of complex TIM systems, where, e.g., individual unit elements are heterogeneous. An example of such a TIM assembly is depicted in Fig. 12(*b*).

2.3 Segmentation. TIM panels can be manufactured as "top-down" in contrast to the bottom-up approach of assembling individual blocks or to 3D printing. In this strategy, the contours of

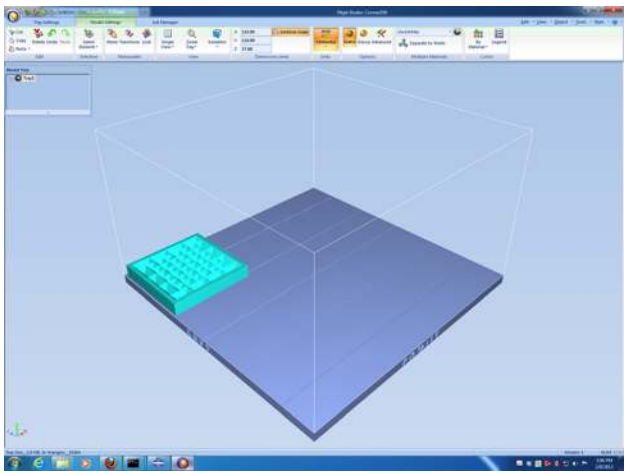

Fig. 11 Three-dimensional printer control software (OBJET STUDIO) for the manufacture of a TIM system.

the blocks are literally carved within a block of monolithic material [44]. This approach is advantageous because the blocks are created in their final position in the panel, and also because it can be implemented on final products or structures already in place, in order to augment their mechanical performance. Now, the surrounding bulk in its unsegmented states provides the in situ scaffold to the TIM system. The approach, however, requires an adequate technology to generate cuts and separate the materials along specific surfaces inside the material. The efficacy of this strategy was recently demonstrated on borosilicate optical glass, using three-dimensional laser engraving. In this case, the methods rely on the transparency of glass to laser light in the near UV range. The three-dimensional laser engraving methods consist in focusing a pulsed laser at a point of predefined location within the volume of glass. While the unfocused laser does not change the structure and properties of glass, the energy concentrated at the focal point is sufficiently high to induce damage, with the prevalent damage mechanism associated to a localized rise of temperature which generates radial microcracks from thermal hoop stresses (Fig. 13(*a*)). The pulsed laser beam can be aimed and focused anywhere within the volume of glass, following predetermined patterns which can be defined using CAD-like package or MATLAB, and which are rapidly created in the material. Arrays of these microcracks form weaker surfaces within the material, and following the concept of "stamp holes," these surfaces can guide cracks along specific predetermined directions and configurations [13,45]. The toughness of the interfaces generated by laser engraving can be finely tuned by adjusting the power of the laser and/or the spacing between the microcracks (Figs. 13(*b*)–13(*d*)), much like the toughness of a line of stamp holes can be adjusted by varying the size and spacing of the holes. Figure 14(*a*) show the configuration of three-dimensional interfaces which were laser engraved within a 50.8×50.8 mm, 3.175 mm thick panel of borosilicate optical grade 263M glass. The weak interfaces define the contours of topologically interlocked blocks, with oblique angle θ. The geometry of the individual blocks was obtained by truncating a tetrahedron which was not necessarily regular in shape, so that TIM panels with different oblique angles for the blocks could be fabricated. These contours were generated numerically using MATLAB (R2014a, MathWorks, Natick, MA), with each block having dimensions $l = 6.375$ mm and $h = 3.175$ mm (Fig. 14(*a*)). The three-dimensional model was then physically engraved within the borosilicate glass panel using a three-dimensional laser engraver (Model Vitrolux, Vitro Laser Solutions UG, Minden, Germany) equipped with a pulsed UV laser (355 nm, 0.5 W cw pumped, 4 kHz repetition rate, and 4–5 ns pulse duration). The method is highly accurate and produces materials with extremely high structural fidelity (Fig. 14(*b*)). Finally, Fig. 14(*c*) shows different materials where blocks with oblique angles from $\theta = 0$ deg to $\theta = 20$ deg were fabricated. The engraved panels were attached to a tape and were loaded in bending at different locations to completely separate each block along the engraved interfaces.

3 Mechanical Response Characteristics

3.1 Quasi-Static Loading. Figure 15 shows a key observation from investigations of the mechanical response of TIM systems under *fixed external confinement* subjected quasi-static loading applied in a transverse direction to the assembly plane. The monolithic equivalent system (a brittle glass plate) fails in a brittle mode with cracks extending throughout the plate; yet, the TIM exhibits a force–deflection response which appears as perfectly damageable [44]. Instead of a sudden drop in the force–deflection response for the brittle monolithic system, the TIM force response smoothly increases and decreases response with the applied deformation. No major cracks are visible in the TIM specimen. Similar findings are documented in Refs. [31], [33], and [46]. In addition to the monotonic loading case, Estrin et al. [31] also considered unloading and partial unloading load paths and reported the finding of a negative elastic modulus.

In order to further investigate the response of TIMs to mechanical loads, several investigators have employed numerical simulation tools. In discrete element simulations [32,46,47], the interaction law between discrete elements is obtained from finite element computations considering only two unit elements, and then, these interaction laws are imparted on the discrete element method (DEM) computation. DEM computations then capture the overall force–deflection response well.

Finite element simulations are computationally more costly than simulations with the respective DEM approach but also provide information on the stress and strain fields in the unit elements, as well as enable one to include failure criteria for the unit elements into the simulation [11,26,28,46,48,49]. An example of such simulation and comparison to the experimental findings is shown in Fig. 16, where the deformed TIM configuration (*a*) is compared to the finite element method (FEM) prediction of the deformed TIM shape (*b*), and the force–deflection data for experiments and simulations are compared (*c*). To obtain such a quantitative agreement between simulation and experiment, an appropriate model parameter calibration has to be conducted [11]. Under the condition that the elastic modulus of the solid in the unit elements is know, the remaining calibration parameters are the (linear) contact stiffness and the (Coulomb) coefficient of friction [29]. The results of a parametric study based on finite element computations demonstrate that the coefficient of friction influences the magnitude of the load-carrying capacity as well as the deflection to final failure. On the other hand, the contact stiffness affects only the load-carrying capacity. Consequently, a calibration procedure can be established by which, first, the coefficient of friction is calibrated with respect to the experimental results of the deflection to final failure, and second, the contact stiffness is tuned to provide the load-carrying capacity in agreement with the experiments.

Several analytical theories have also been presented to predict the observed deformation response of TIMs to transverse mechanical loads. Estrin and coworkers extend classical beam [23] or plate [50] theories to TIM systems by introducing partial through-thickness cracks. Thereby, the lack of load transfer through part of the TIM thickness is accounted for. On the other hand, such an approach still assumes some tensile stresses in the remaining uncracked ligament. Such tensile stresses would, however, not exist in a TIM where load transfer between unit elements is by contact only. Brocato and Mondardini [21] used a strain energy approach to derive the force–deflection response of TIM-like systems. Yet, their approach assumes bending of unit elements as the mayor contribution to deformation. Such deformation mode would not be dominant for TIMs as those discussed in the present paper where unit elements are restricted to aspect ratios of unity. In Ref. [33], a model based on concepts of post-tensioned masonry walls was applied to TIMs. Thereby, TIM failure was analyzed and

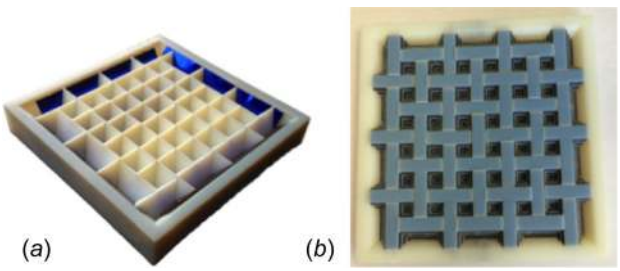

Fig. 12 (*a*) A homogeneous 3D-printed TIM. Metal shim stock is used along the frame to control confinement pressure in the assembly. (*b*) A 3D-printed TIM with microstructured unit elements, unit elements are truncated tetrahedra.

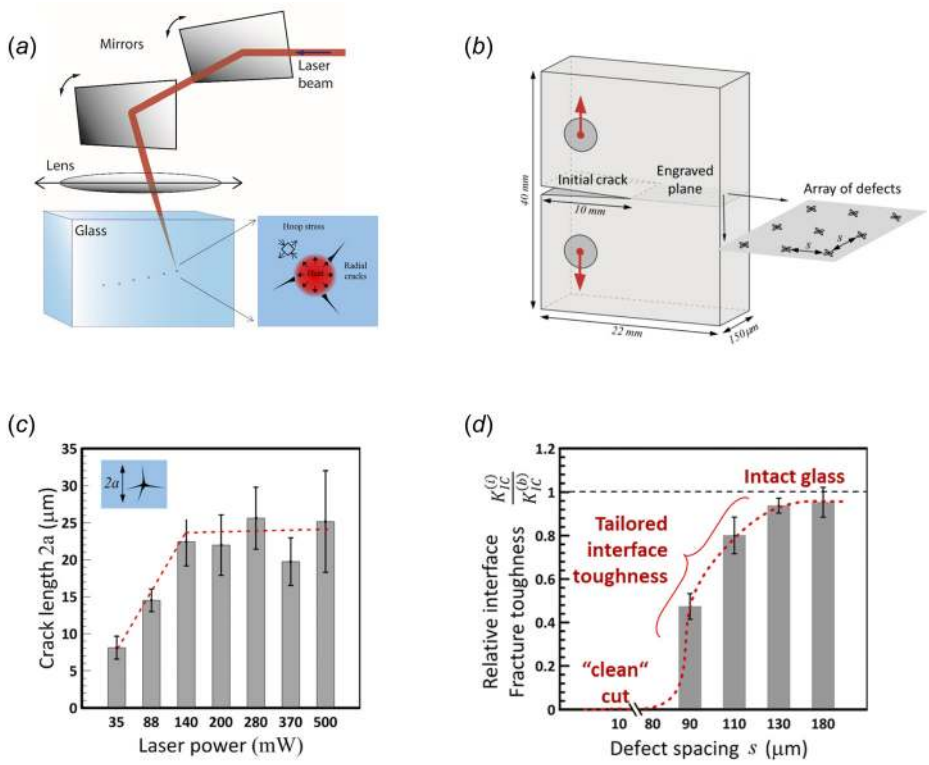

Fig. 13 Generating weak interfaces within glass: (*a*) a nanosecond-pulsed laser focused beam creates microdefects at its focal point. Arrays of these defects define the weak interfaces between individual blocks. (*b*) Glass compact tension specimen used to measure the toughness of the laser-engraved interface; (*c*) the size of the defects can be adjusted by the power of the laser; and (*d*) the toughness of the interfaces can be tuned from zero ("laser cutting") to the toughness of bulk glass by adjusting the spacing between defects [13,45] (original figures by the authors).

predicted as an outcome of unit element strength and the geometry of the material architecture. This model was, however, not applied to predict the force–deflection response. As an alternative, Khandelwal et al. [28] proposed a model where load transfer internal to a TIM occurs by compression only and along thrustlines [14,51,52]. For the remainder of this paper, this approach is referred to as the *thrustline deformation* (TD) theory of TIMs. In the TD theory, the overall nonlinear mechanical response of a TIM (under transverse loading) emerges as a consequence of geometrical nonlinearity of the internal thrustline structure.

Figures 17(*a*) and 17(*b*) depict the computed distribution of the maximum compressive principal stress in a TIM under transverse

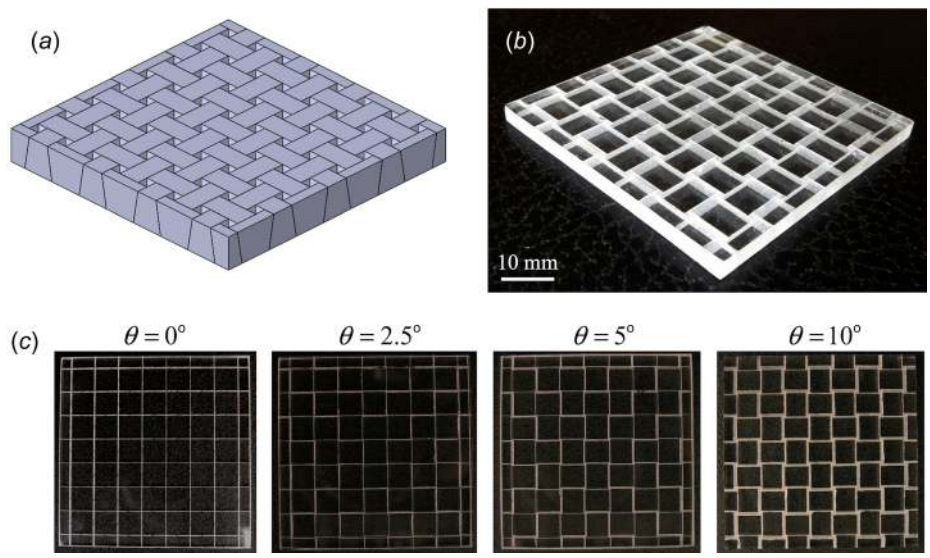

Fig. 14 Architectured glass panels: (*a*) numerical models where the interfaces define and array of truncated tetrahedra which are topologically interlocked, (*b*) picture of the laser-engraved panel, and (*c*) top view of four engraved panels with different oblique angles. (Reproduced with permission from Mirkhalaf et al. [44]. Copyright 2016 by Elsevier.)

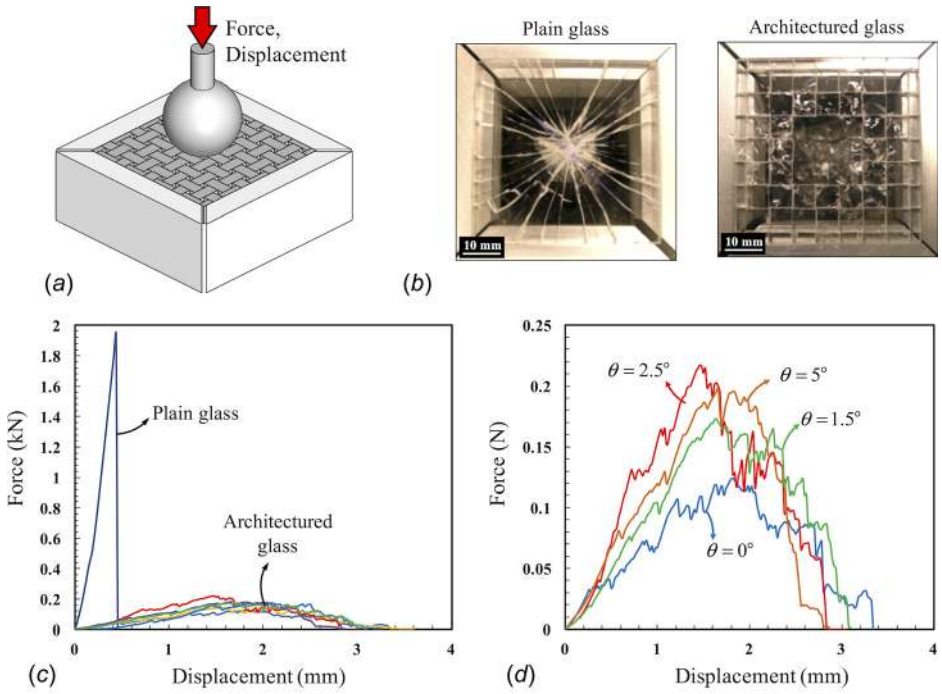

Fig. 15 Quasi-static force–deflection response of transversely loaded TIM assembly and comparison to a monolithic equivalent: (*a*) schematic of experiment, (*b*) failure pattern in plain glass and architectured glass, (*c*) force–displacement response measured for plain glass and architectured glass, and (*d*) force–displacement response measured for several different architectured glass segmentation angles. (Reproduced with permission from Mirkhalaf et al. [44]. Copyright 2016 by Elsevier.)

loading. Figure 17(*c*) depicts the substitution of the thrustline with the truss structure. In the TD theory, the force–deformation response of a TIM is then computed as the response of the equivalent truss structure emerging from the thrustlines. This recognizes the discrete nature of the TIM and the relevance of the compression-only load transfer across the unit-to-unit contacts. The load-carrying capacity of the TIM is limited by an internal instability process inherent in the equivalent truss structure. Individual thrustlines (i.e., equivalent trusses) sequentially go through an instability process similar to that occurring in a van Mises truss. Accounted for in its sequential nature, this sequence of instability events allows one to understand the failure response as an instability processes. Considering a linear TD theory, each thrustline carries in-plane f_H and out-of-plane f_V forces

$$f_H = \eta a_0^2 E \frac{(2R_{p,0} + a_0) - (2r + a)}{2R_{p,0}/\cos\xi + a_0} \quad f_V = f_H \tan\xi \quad \tan\xi = \frac{h - \delta}{l_0 + \frac{f_H}{2E\eta a_0}} \tag{1}$$

where $R_{p,0}$, a_0 and r, a define the equivalent truss length and unit element size in the undeformed deformed state, respectively. The angle ξ defines the inclination of the thrustline to the plane in dependence of the displacement δ_i at the center of the thrustline system. In using this formulation for TIM, it is considered that no load transfer can take place in tension. The segmentation angle θ will determine the virtual cross section of the thrustline ηa_0^2. The dependence of η on θ reflects the type of segmentation. The overall force F deflection response is then

$$F = \sum_i^N f_{Hi}(\delta_i) \tag{2}$$

indicating that each TIM configuration possesses N thrustlines locally experiencing an applied displacement δ_i. The local δ_i is related to the overall applied displacement δ assuming a linear kinematic relationship between the externally applied displacement δ and the displacement applied to each individual thrustline δ_i. The elastic response of individual unit elements is linear and represented by the elastic modulus E. The segmentation characteristics of the TIM as expressed by the angle θ (Fig. 14) are captured by the parameter η which defines an effective unit-to-unit contact area. The TD model predictions are in good agreement with the full-field FE models [38]. In computational models, we have accounted for more details such as friction, assembly

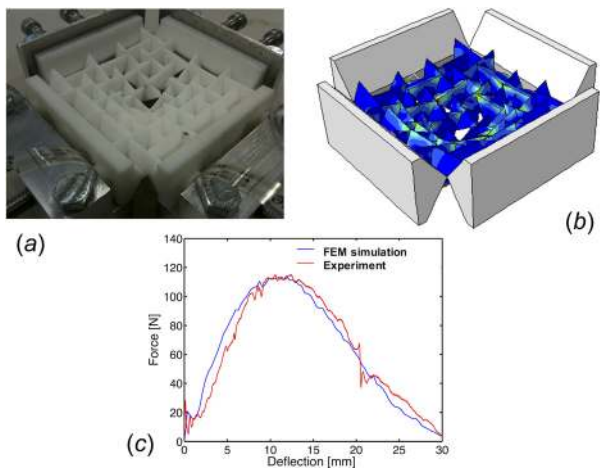

Fig. 16 (*a*) TIM in deformed configuration due to transverse loading, (*b*) predicted deformed configuration and spatial distribution of Mises equivalent stress, and (*c*) measured and predicted force–deflection response. (Reproduced with permission from Feng et al. [11]. Copyright 2015 by Elsevier.)

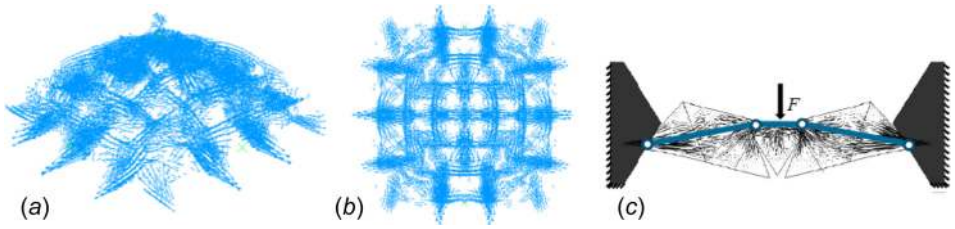

Fig. 17 Distribution of compressive principal stresses in TIM under transverse load ((*a*) and (*b*)); from thrustline to truss system (*c*).

tolerances, and damage via the cohesive zone model approach. Both models were tested successfully by experiments [28].

The damage tolerance of TIMs has been attributed to the crack-arresting capacity of the contact interfaces between individual unit elements [24], favorable statistical size effects [1], and crack percolation [41]. Crack formation in individual unit elements is not a necessary process for failure of TIMs. The TD deformation theory attributes failure of TIMs and the apparent damage tolerance not to fracture processes in the unit elements but primarily to a sequence of material internal instabilities. Since TIM failure is a consequence of instability, and not dominantly associated with the degradation of the material use in the TIM, it was shown in Ref. [33] that a failed TIM can be reassembled and reused without a significant loss of properties. The mechanical properties of reused TIMs were shown to be nearly fully recoverable by substituting the only few unit elements which had sustained damage in prior loading.

The type of constraint used to confine the unit elements of the TIM system was found to determine the mechanical response [53]. Figure 18 compares the mechanical response under transverse loading of TIM with a fixed and rigid external confinement (Fig. 12(*a*)) to that of a TIM with internal confinement (Fig. 9(*a*)). Both TIM systems are made of the same unit elements. In the internally constraint system, the mechanical response emerges from the interaction of the TIM unit elements with the internal constraining fiber or tow material. While the externally confined TIM gradually softens, the internally confined TIM gradually stiffens. Such stiffening mechanical response of the internally confined TIM is similar to that of a tensegrity structures (a quadratic, nonlinear stiffness). The internally confined TIM with tensile-carrying fibers or tows is thus termed a tensegrity TIM. For the tetrahedra-based TIM system with the limit case where the weave is the main load-carrying component and the TIM units primarily provide the geometrical guidance for the weave, the nonlinear elastic force F deflection δ response follows from adaptation of the tensegrity model by Calladine [54]

$$F \sim E_f A_f \left(\frac{\delta}{L_0}\right)^3 \tag{3}$$

where E_f is the modulus, A_f is the cross section of the fiber, and L_0 is the in-plane extension. This approach fits the elastic experimental data of Fig. 18 well.

Past the strength of the tensegrity TIM, multiple processes of strength recovery were observed (Fig. 17). This effect is attributed to the fact that the stored energy in the filaments can be used to close a puncture-type failure locally. Similarly, residual stress-based mechanisms have been cited as responsible for wound closure in tissue [55–57].

3.2 Impact Loading. Under impact loading, the resistance to impact, the damage tolerance, and the coefficient of restitution (or the residual velocity of the impactor) are of concern. Impact experiments on glass-based systems have demonstrated that the architectured TIM glass is both impact resistant and damage tolerant (Fig. 19). When compared to an equivalent monolithic glass panel, the TIM systems possess not only the higher impact energy to initiate failure but also a higher coefficient of restitution. Specifically, the TIM glass system manufactured by the laser-scribing processes could resist two to four times more impact energy compared to panels made of plain glass [44]. To obtain optimum performance, the oblique angle θ must be finely adjusted. In the present case, TIM glass panels with $\theta = 2.5$ deg produced the highest resistance to impacts [44]. Yet, such an optimization poses no fundamental challenge to the manufacturing approach. In the monolithic reference system, the damage is widespread with cracks initiating at the impact site spreading to the system boundary. For the TIM, however, the damage is locally confined to the impact site.

Computational simulations of the impact response of a TIM system were conducted for models where the TIM unit elements are elastic solid and for cases where the TIM unit element model domain is enhanced by cohesive zone elements [11]. Results from the computations including the cohesive elements and simulating the impact loading are shown in Fig. 20 where the failure due to impact for a TIM and the equivalent monolith are depicted. Model simulations used in these computations are documented in Ref. [11], and the cohesive zone properties are: cohesive strength $\sigma_{\max} = E_0/100$, cohesive length to full material separation $\delta_f = a_0/1000$, and cohesive length to maximum cohesive traction $\delta_c = \delta_f/10$. The cohesive zone structure is imposed a priori (ten segments along the edge of a tetrahedron). The simulations are in good qualitative agreement with the experiments shown in Fig. 19. In the TIM case, the damage is confined to the domain around the impactor and in that region significant fragmentation is observed. Fragments are ejected from the TIM, and the kinetic energy is transferred from the impactor to

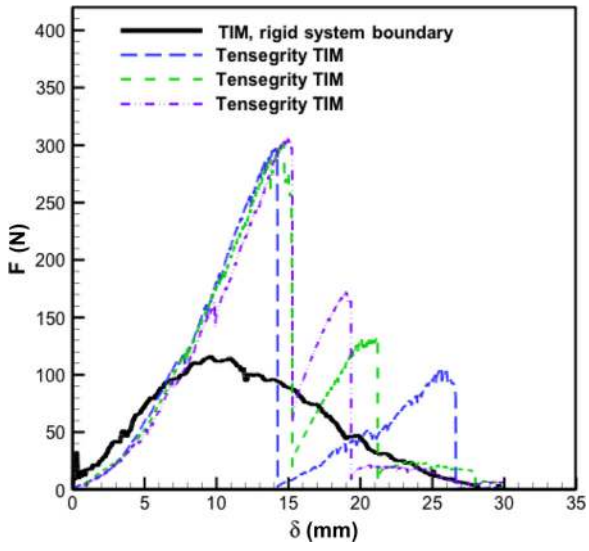

Fig. 18 Representative force–deflection curves for transversely loaded TIM assemblies with rigid external constraint and internal constraint by carbon fiber tow [53].

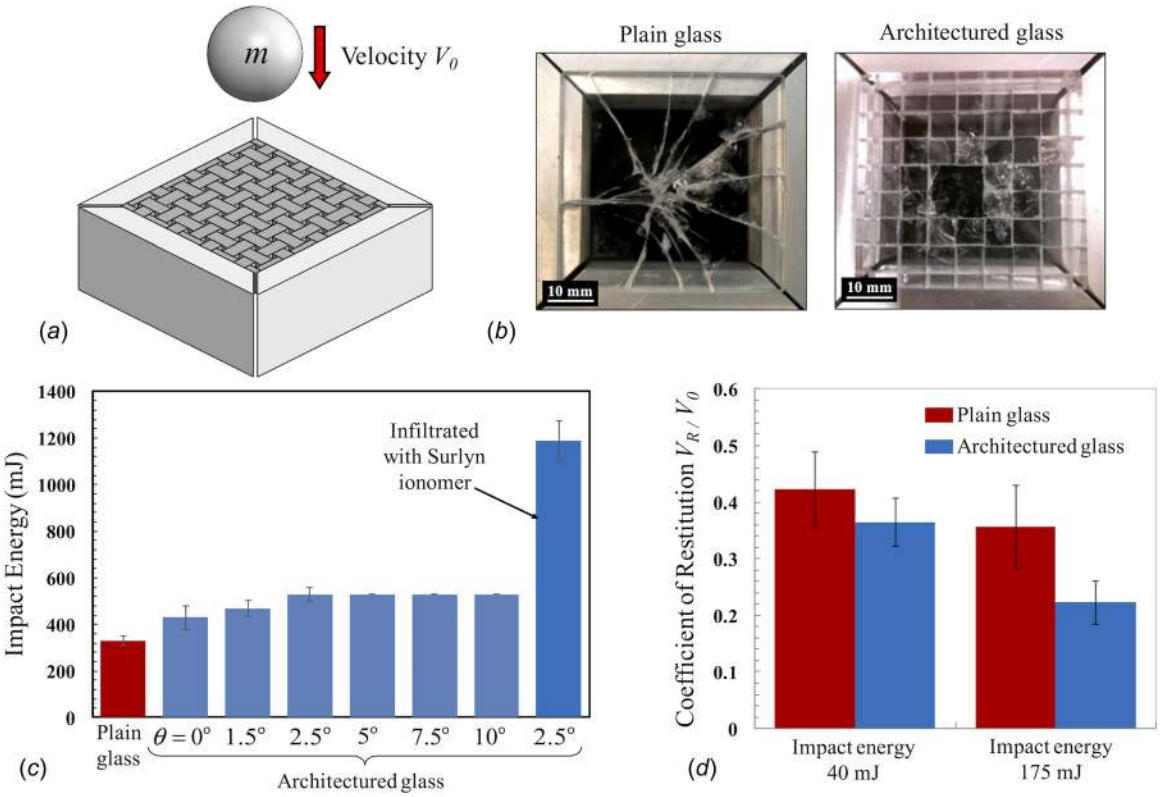

Fig. 19 Impact characteristics for a glass-based TIM: (*a*) schematic of experimental setup, (*b*) failure pattern in plain glass and architectured glass, (*c*) impact energy of architectured glasses, modified architectured glasses, and plain glass, and (*d*) coefficients of restitution of architectured glass and plain glass. (Reproduced with permission from Mirkhalaf et al. [44]. Copyright 2016 by Elsevier.)

the ejected fragments. On the other hand, in the monolithic case, the damage is widespread and reaches the system boundary. The amount of ejected fragments is small. In addition, a full set of residual velocity computations was performed for a TIM model with elastic elements, excluding damage to the unit elements. The resulting Lambert–Jonas (LJ) plot is shown in Fig. 21. The residual impactor velocity response was found to deviate from the response commonly observed for monolithic materials. The residual velocity, v_{res}, for an impact velocity of v_{im} is commonly fitted to the LJ relationship [58]: $v_{res} = c(v_{imp}^p - v_{bl}^p)^{(1/p)}$, where v_{bl} is the ballistic velocity and c and p are considered as material constants. For the TIM simulation, it was found that two domains exist, each

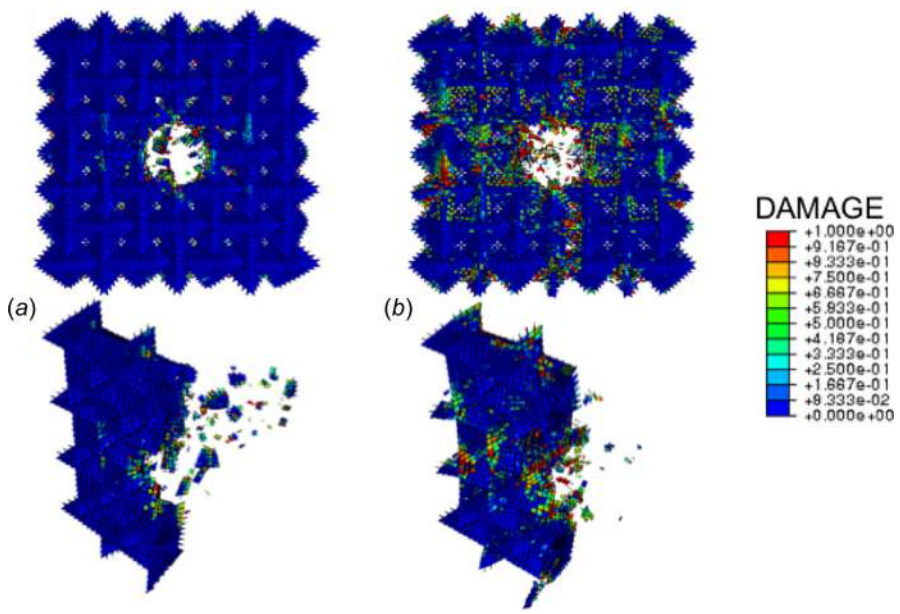

Fig. 20 Finite element simulation of impact on (*a*) damage distribution in a TIM system and (*b*) damage evolution in the equivalent monolithic system. Simulations account for cohesive elements distributed evenly throughout the model volume.

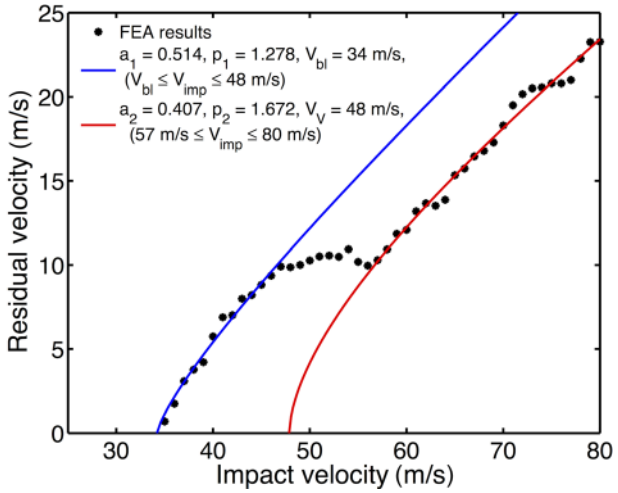

Fig. 21 LJ relationship for a TIM, computational prediction. (Reproduced with permission from Feng et al. [11]. Copyright 2015 by Elsevier.)

described by a unique set of parameter values in the LJ relationship and an intermediate transition (Fig. 21). The parameter p in high-velocity regime for TIMs was similar as for conventional metallic plates, but for the low-velocity regime close to the ballistic limit was found to be much smaller than in conventional metallic plates. In the low-velocity regime, a strong projectile–TIM interaction exists, and the in-plane confinement forces remain high throughout the impact event leading to a desirable low value of p. At a high impact velocity, the impact leads to a rapid loss of in-plane confinement and thus a weak projectile–TIM interaction, and consequently a larger p value.

3.3 Active TIM Systems. Confinement of the TIM plays an important role in defining the mechanical response of the TIM. In that sense, the TIM systems are not unlike granular materials. Since there is no restriction that the external rigid system boundary needs to be fixed in space during loading, the mechanical response of TIMs can actively be controlled.

In Ref. [35], the authors employ active and adaptive control of the external constraints to achieve variable stiffness, including negative stiffness. This study furthermore demonstrates that active control allows to hold the force constant over a large range of transverse deflection. Such a response is desirable for packaging and protection applications where energy dissipation at a controlled load level is needed. In cellular solids, which are often used for such applications, this goal is achieved by controlling the buckling processes in the cell walls. In TIMs, instead, the response is achieved by active control such that the plateau stress level can be adjusted adaptively to the desired impact load (Fig. 22(*a*)). Cellular solids also have the drawback that after exceeding the densification strain, the stress level increases strongly. In TIMs, instead, the load can be controlled and ramped down to lower levels (Fig. 22(*b*)). The combination of controlled high stiffness and energy absorption is a unique feature to TIM systems.

In Ref. [34], it was shown that the control of the constraint can not only be achieved by controlling the constraint conditions through externally prescribed displacement of the rigid system boundary but also that the constraint can be changed in an autonomous way. In Ref. [34], shape memory wires embedded through channels in the unit elements span between the rigid system boundaries. Activation of the shape memory alloy (SMA) effect leads to a contraction/expansion of the SMA wires and a change in constraint such that under constant transverse deflection, the resistance of the TIM is controlled. Figure 23 depicts the TIM embodiment with unit cells as osteomorphic blocks and SMA wires, as well as an example of the displacement and force response under SMA current on/off control.

The control of TIMs by embedded fibers or wires has also been extended to the internally confined TIMs shown in Fig. 9. Thereby, the C-fiber tow is augmented by an SMA wire. Furthermore, the TIM unit elements are considered as unilaterally truncated tetrahedra, which introduces an asymmetry into the bending resistance. Also, since the SMA wire is guided by the line of sight in the TIM assembly, the C-fiber tow weave and the SMA wire are located off-center. As a consequence, a moment is introduced by the contraction of the SMA wire once the current is switched on, and the TIM cantilever deflects. The results of such experiments are shown in Fig. 24. The observed time scale of the active response was found to be well in line with that of other SMA-driven systems. The maximum deflection attainable was found to scale linearly with the truncation percentage.

4 Summary and Outlook

The present paper demonstrates manufacturing processes for TIMs and discusses aspects of their mechanical properties.

The use of a *scaffold* emerges as a unifying theme across all processes considered for both bottom-up assemblies and top-down

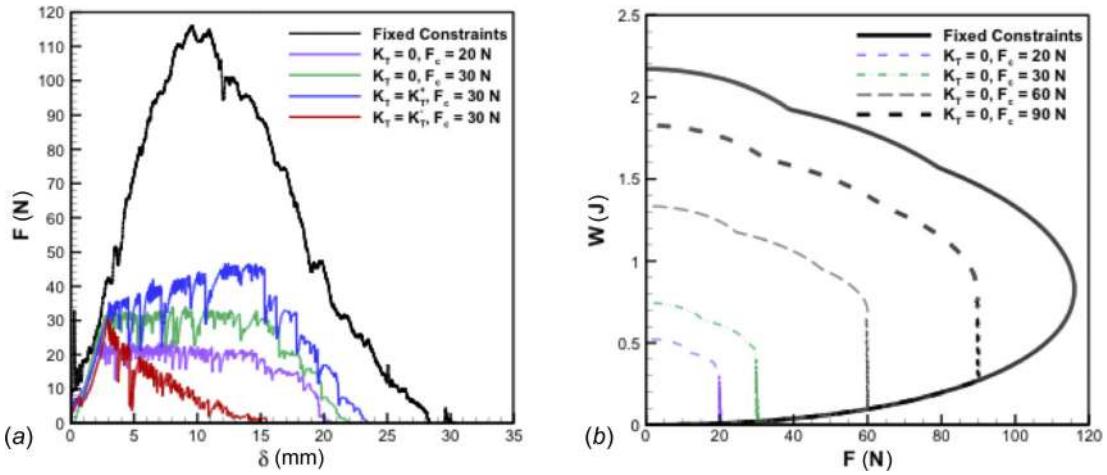

Fig. 22 Control of mechanical response of a TIM through the in-plane constraint: (*a*) TIM force–deformation response under control of the external constraint, positive, and negative stiffness is achieved. (*b*) Predicted energy absorption diagram considering several actively controlled TIM cases with several plateau load values. (Reproduced with permission from Khandelwal et al. [35]. Copyright 2015 by IOP Publishing Limited.)

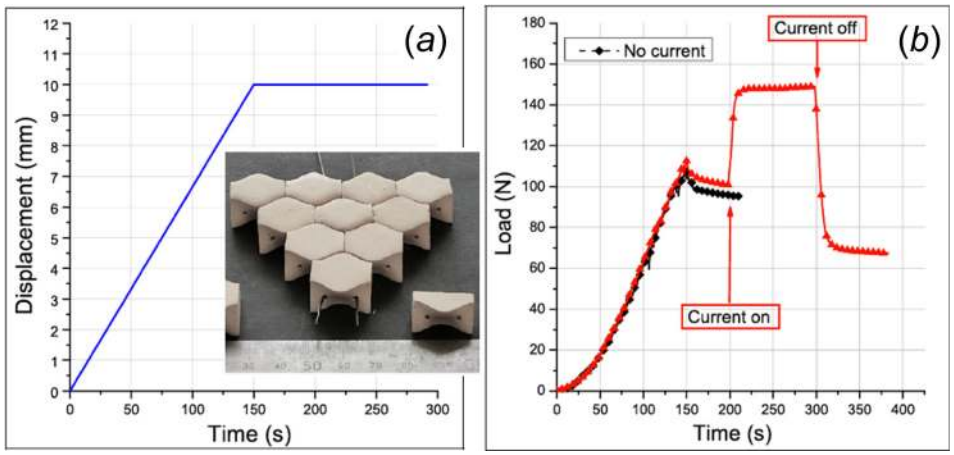

Fig. 23 Control of mechanical response of a TIM by embedded SMA wires controlling the in-plane constraint: (*a*) imposed transverse displacement, insert depicts the TIM system composed of osteomorphic bricks and the SMA wires in channels through the brick units; (*b*) response of the SMA-enhanced TIM to SMA current during constant applied displacement. The current alters in in-plane constraint and thus the stiffness of the TIM. (Reproduced with permission from Molotnikov et al. [34]. Copyright 2015 by IOP Publishing Limited.)

segmentation approaches. Scaffolds for TIM assemblies are inscribed with the underlying lattice of the TIM and the specific positioning information for the individual unit elements of the assembly.

A series of bottom-up approaches has been considered. Rigid scaffolds were shown in the context of a gravity and robotic assembly. The gravity-assisted assembly approach has been the method used to assemble stereotomy-based structures through the ages and was recently reported as the method of choice for the assembly of topologically interlocked wall structures [40]. The experience of the authors is that this method is also viable for assembles with large number of unit elements but requires user interference to correct the position incorrectly located unit elements, especially when considering assemblies with a large number of individual elements. Clearly, individual unit elements possess large weight as in building construction, this approach is preferred. The assembly on a planar scaffold was demonstrated with the use of a robotic arm and end-effector. Such approaches are also relevant for periodic assemblies of platonic solids other than the tetrahedra. The relevant template obviously is directly related to the TIM system considered. For example, for TIM assemblies of cubes [26], the template is of hexagonal symmetry, and the assembly requires three in-plane directions of motion in the placement of the cube unit elements. Osteomorphic brick systems [27] or assemblies of truncated tetrahedra (Fig. 14) could be assembled on flat template, but the directionality of the assembly processes remains identical to that described here. Tessmann [16] demonstrated TIM systems with nonplanar geometries such that the nonplanar assembly templates are naturally needed. Flexible scaffolds were considered such that the scaffold itself becomes a part of the final *hybrid* TIM. This approach was demonstrated conceptually for the case of TIM-based sandwich panels where the scaffold plane becomes the facesheet of the composite. A deformable scaffold was demonstrated to enable the parallel assembly of a TIM. The deformable scaffold shown is based on a string grid. The resulting TIM can be considered as composite material

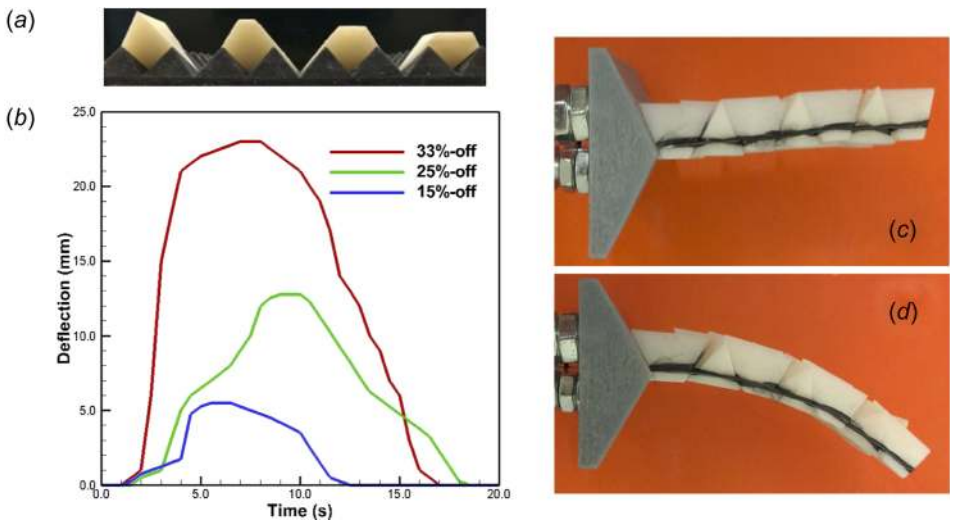

Fig. 24 Shape morphing TIM system: unilaterally truncated tetrahedra units (0–33%) (*a*) are used to construct internally constraint TIMs (Fig. 9(*b*)) with part of the C-fiber tow augmented by an SMA wire. The resulting TIM deflection is controlled by the SMA wire (*b*) and allows to control the shape from flat (*c*) to curved (*d*).

system with continuous fibers in a weave embedded in a discontinuous matrix. For the self-assembly of tetrahedra into the TIM, structure-specific considerations regarding the orientation and mobility of the tetrahedra were required. The liquid-associated buoyancy provides the scaffold and mobility at the same time while the positioning of magnets encodes the assembly template. For osteomorphic bricks or truncated tetrahedra, the mobility needed for self-assembly processes can be alternatively achieved by the use of low-friction surfaces in combination with vibration, or with air-tables where the air flow per nozzle is altered spatiotemporal. Magnetic elements can be seen as sacrificial, but can also become active elements and for the basis for control of stiffness and damping. Overall, in the experience of the authors, the method of self-assembly is difficult to control, and achieving a well-ordered structure has proven to be challenging. The 3D printing approach to the manufacturing of TIM system provides a unique opportunity to control both geometry and microstructure at the same time. This approach poses no limit to alteration in geometry of the unit elements and of the material in the unit elements. Sacrificial scaffolds are common to 3D print processes and enable the integrated manufacture of the TIM with its constraints. The top-down segmentation approach documented here is unique in that the scaffolding is in situ. This enables to locate segmented domains in arbitrary locations in a monolithic material, and to tailor the segmentation interfaces in their strength to the specific application under consideration.

TIM systems present an opportunity to expand the available material property space and provide material solutions with enhanced interesting and adaptable deformation characteristics, damage tolerance, dynamic, and acoustical properties. This paper reviews key aspects of quasi-static and impact loading response. The key features that emerge are that load transfer in TIMs emerges as best be described by an approach that explicitly accounts for the discrete nature of the microstructure. This is both the case in numerical simulations with the discrete element method and the finite element method as well as in analytical approaches. The mechanical response is then a result of internal instability processes rather than the stress–strain response of the solids used to make the unit elements. This finding appears to hold for both TIMs confined externally as well as internally.

TIM systems are reviewed in the context of manufacturing processes and related aspects of mechanical properties. While the present paper reports on material systems built from unit elements with size of on the millimeter and centimeter scale, there are no principal limitations to consider small- and larger-sized unit elements. Yet, at the same time, specific additional considerations will be needed in both manufacturing processes and regarding mechanical properties. For example, for micro- and nanometer size unit elements, attractive surface interaction forces between unit elements become relevant. Such forces can enhance self-assembly, but would make other assembly processes more difficult. Such attractive surface interactions would also contribute to the mechanical response of TIMs under external loads by adding a tensile component to the particle interaction and thereby leading to potentially enhanced strength and toughness [23] as well as impact resistance (Fig. 19). On the other hand, and TIM systems made of unit elements of meter size have been considered in building applications. Self-weight of the unit elements then leads to a selection of manufacturing processes which actively employ self-weight [40]. In the mechanical response, self-weight then exceeds that of external loads [15–17].

TIM system has been proposed as solutions to a range of engineering material problems. What readily emerges from the unique deformation response to transverse loading is the use of TIMs in protective layers or coatings [23]. This integration into an engineered product has been demonstrated in Ref. [59]. In protective materials, lightweighting is often desired and fully dense unit elements in TIMs might not provide an ideal configuration. In Ref. [28], it was demonstrated that the use of cellular unit elements is readily possible. The desirable energy dissipation characteristics are not only relevant to quasi-static loading but have (at least from a simulation viewpoint) also been demonstrated for impact loading [11]. The damage tolerance was found to be further enhanced in the tensegrity-type TIM systems where self-healing type processes have been documented [53]. Contact interactions bring a range of nonlinear features into the dynamic response, and such properties have been exploited in acoustic applications [36,37]. Architectured such material solutions often enable new multifunctionalities where materials are not only selected for their mechanical properties but also for functional properties [1,38]. Considering the topologically engraved glass system described in Refs. [13], [44], and [45], relevant applications can be envisioned where optical performance together with toughness and impact resistance is desired, such as glass panels for application in resilient buildings, in safety glass for transportation applications, light fixtures, or touch screens. At high-temperature, ceramics often provide the only path to achieve thermal protection, but ceramics are often far too brittle and lack damage tolerance. TIMs have been proposed as alternatives to conventional tile assemblies for such applications [39,60]. Considering aspects of sustainability as a functionality, TIMs—due to the spatial confinement of damage—then provide a path leading to the implementation of reusable engineering material systems. Responsive TIMs [34,35] can form the basis for smart energy absorbing material systems. Based on such approaches, adaptive packaging material can be envisioned, which adaptively can be changed to conform to the present object to be protected. The capability to switch from high primary stiffness to low secondary stiffness is desirable in catching mechanisms where the primary response enables tight position control and the secondary response enables controlled energy absorption. The absence or presence of a binder in TIM systems needs to be carefully considered. For some application scenarios, such as high-temperature applications [39,60], remanufacturing [33], or even extraterrestrial construction [61], binderless systems are desirable. In these cases, TIM has mostly relied on frictional interaction between the blocks to generate attractive properties at the macroscale. It is conceivable that the mechanics of stress transfer at the interface can be further tailored and optimized by using a binder [23] such as a polymeric adhesive. The potential of this approach has been recently demonstrated on architectured glass panels where the blocks were glued by a ductile polymer (Surlyn ionomer). The effect was to double the impact resistance of the materials (Fig. 12, in Ref. [44]). Hard biological materials such as seashell, teeth, or bone can, in many ways, be interpreted as dense architectured materials [62,63]. The mechanisms of stress transfer at the many interfaces that these materials contain are governed by the deformation of thin proteins layers which include the formation of ligaments and the unfolding of individual molecules, or the dynamic breakage and formation of hydrogen bonds [64]. These highly sophisticated features could serve as inspiration and models for the developed of tailored interfaces in synthetic architectured materials and further expand the potential application domains of the TIM systems reviewed in this article.

Acknowledgment

T.S. acknowledges the funding by the Army Research Office (Grant Mechanics of Multiscale Energy Dissipation in Topologically Interlocked Materials-11.1 STIR), T.S. and R.J.C. acknowledge the funding via AFOSR (Grants FQ8671-090162 and FA2386-12-1-3020), as well as the Indiana 21st Century Research and Technology Fund. The work of F.B. was supported by an I2I grant from the Natural Sciences and Engineering Research Council of Canada and by the Fonds de Recherche du Quèbec—Nature et Technologies. The contributions by A. Anderson (on self assembly) and Z. Wu (on active systems) are gratefully acknowledged.

References

[1] Ashby, M. F., and Bréchet, Y. J. M., 2003, "Designing Hybrid Materials," Acta Mater., **51**(19), pp. 5801–5821.

[2] Ashby, M. F., 2005, "Hybrids to Fill Holes in Material Property Space," Philos. Mag., **85**(26–27), pp. 3235–3257.
[3] Bouaziz, O., Bréchet, Y., and Embury, J. D., 2008, "Heterogeneous and Architectured Materials: A Possible Strategy for Design of Structural Materials," Adv. Eng. Mater., **10**(1–2), pp. 24–36.
[4] Ashby, M. F., 2011, "Hybrid Materials to Expand the Boundaries of Material-Property Space," J. Am. Ceram. Soc., **94**(s1), pp. s3–s14.
[5] Fleck, N. A., Deshpande, V. S., and Ashby, M. F., 2010, "Micro-Architectured Materials: Past, Present and Future," Proc. R. Soc. A, **466**(2121), pp. 2495–2516.
[6] dell'Isola, F., Steigmann, D., and Della Corte, A., 2015, "Synthesis of Fibrous Complex Structures: Designing Microstructure to Deliver Targeted Macroscale Response," ASME Appl. Mech. Rev., **67**(6), p. 060804.
[7] Bertoldi, K., Boyce, M. C., Deschanel, S., Prange, S. M., and Mullin, T., 2008, "Mechanics of Deformation-Triggered Pattern Transformations and Superelastic Behavior in Periodic Elastomeric Structures," J. Mech. Phys. Solids, **56**(8), pp. 2642–2668.
[8] Nesterenko, V. F., 2001, *Dynamics of Heterogeneous Materials*, Springer Science & Business Media, New York.
[9] Porter, M. A., Kevrekidis, P. G., and Daraio, C., 2015, "Granular Crystals: Nonlinear Dynamics Meets Materials Engineering," Phys. Today, **68**(11), pp. 44–50.
[10] Gu, X. W., and Greer, J. R., 2015, "Ultra-Strong Architected Cu Meso-Lattices," Extreme Mech. Lett., **2**, pp. 7–14.
[11] Feng, Y., Siegmund, T., Habtour, E., and Riddick, J., 2015, "Impact Mechanics of Topologically Interlocked Material Assemblies," Int. J. Impact Eng., **75**, pp. 140–149.
[12] Molotnikov, A., Gerbrand, R., Bouaziz, O., and Estrin, Y., 2013, "Sandwich Panels With a Core Segmented Into Topologically Interlocked Elements," Adv. Eng. Mater., **15**(8), pp. 728–731.
[13] Mirkhalaf, M., Dastjerdi, A. K., and Barthelat, F., 2014, "Overcoming the Brittleness of Glass Through Bio-Inspiration and Micro-Architecture," Nat. Commun., **5**, p. 3166.
[14] Heyman, J., 1966, "The Stone Skeleton," Int. J. Solids Struct., **2**(2), pp. 249–279.
[15] Tessmann, O., and Becker, M., 2013, "Extremely Heavy and Incredibly Light: Performative Assemblies in Dynamic Environments," Open Systems: Proceedings of the 18th International Conference on Computer-Aided Architectural Design Research in Asia (CAADRIA 2013), The Association for Computer-Aided Architectural Design Research in Asia (CAADRIA), Hong Kong, and Center for Advanced Studies in Architecture (CASA), Department of Architecture, National University of Singapore, Singapore, May 15–18, pp. 469–478.
[16] Tessmann, O., 2012, "Topological Interlocking Assemblies," Physical Digitality—Proceedings of the 30th International Conference on Education and Research in Computer Aided Architectural Design in Europe, Prague, Czech Republic, Sept. 12–14, Vol. 2, pp. 211–220.
[17] Rippmann, M., and Block, P., 2013, "Rethinking Structural Masonry: Unreinforced, Stone-Cut Shells," Proc. Inst. Civ. Eng.: Constr. Mater., **166**(6), pp. 378–389.
[18] Conway, J. H., and Torquato, S., 2006, "Packing, Tiling, and Covering With Tetrahedra," Proc. Natl. Acad. Sci., **103**(28), pp. 10612–10617.
[19] Kanel-Belov, A. J., Dyskin, A. V., and Estrin, Y., 2010, "Interlocking of Convex Polyhedra: Towards a Geometric Theory of Fragmented Solids," Moscow Math. J., **10**(2), pp. 337–342.
[20] Weizmann, M., Amir, O., and Grobman, Y. J., 2015, "Topological Interlocking in Architectural Design," Emerging Experience in Past, Present and Future of Digital Architecture—Proceedings of the 20th International Conference of the Association for Computer-Aided Architectural Design Research in Asia (CAADRIA 2015), Daegu, South Korea, May 20–22, The Association for Computer-Aided Architectural Design Research in Asia (CAADRIA), Hong Kong, pp. 107–116.
[21] Brocato, M., and Mondardini, L., 2015, "Parametric Analysis of Structures From Flat Vaults to Reciprocal Grids," Int. J. Solids Struct., **54**, pp. 50–65.
[22] Glickman, M., 1984, "The G-Block System of Vertically Interlocking Paving," 2nd International Conference on Concrete Block Paving, Delft University of Technology, Apr. 10–12, American Society for Testing and Materials, Delft, The Netherlands, pp. 345–348.
[23] Dyskin, A. V., Estrin, Y., Kanel-Belov, A. J., and Pasternak, E., 2001, "A New Concept in Design of Materials and Structures: Assemblies of Interlocked Tetrahedron-Shaped Elements," Scr. Mater., **44**(12), pp. 2689–2694.
[24] Dyskin, A. V., Estrin, Y., Kanel-Belov, A. J., and Pasternak, E., 2001, "Toughening by Fragmentation—How Topology Helps," Adv. Eng. Mater., **3**(11), pp. 885–888.
[25] Dyskin, A. V., Estrin, Y., Kanel-Belov, A. J., and Pasternak, E., 2003, "Topological Interlocking of Platonic Solids: A Way to New Materials and Structures," Philos. Mag. Lett., **83**(3), pp. 197–203.
[26] Schaare, S., Dyskin, A. V., Estrin, Y., Arndt, S., Pasternak, E., and Kanel-Belov, A., 2008, "Point Loading of Assemblies of Interlocked Cube-Shaped Elements," Int. J. Eng. Sci., **46**(12), pp. 1228–1238.
[27] Krause, T., Molotnikov, A., Carlesso, M., Rente, J., Rezwan, K., Estrin, Y., and Koch, D., 2012, "Mechanical Properties of Topologically Interlocked Structures With Elements Produced by Freeze Gelation of Ceramic Slurries," Adv. Eng. Mater., **14**(5), pp. 335–341.
[28] Khandelwal, S., Siegmund, T., Cipra, R. J., and Bolton, J. S., 2012, "Transverse Loading of Cellular Topologically Interlocked Materials," Int. J. Solids Struct., **49**(18), pp. 2394–2403.
[29] Autruffe, A., Pelloux, F., Brugger, C., Duval, P., Bréchet, Y., and Fivel, M., 2007, "Indentation Behaviour of Interlocked Structures Made of Ice: Influence of the Friction Coefficient," Adv. Eng. Mater., **9**(8), pp. 664–666.
[30] Dyskin, A. V., Pasternak, E., and Estrin, Y., 2012, "Mortarless Structures Based on Topological Interlocking," Front. Struc. Civ. Eng., **6**(2), pp. 188–197.
[31] Estrin, Y., Dyskin, A. V., Pasternak, E., Schaare, S., Stanchits, S., and Kanel-Belov, A. J., 2004, "Negative Stiffness of a Layer With Topologically Interlocked Elements," Scr. Mater., **50**(2), pp. 291–294.
[32] Brugger, C., Bréchet, Y., and Fivel, M., 2008, "Experiments and Numerical Simulations of Interlocked Materials," Adv. Mater. Res., **47–50**, pp. 125–128.
[33] Mather, A., Cipra, R. J., and Siegmund, T., 2012, "Structural Integrity During Remanufacture of a Topologically Interlocked Material," Int. J. Struct. Integr., **3**(1), pp. 61–78.
[34] Molotnikov, A., Gerbrand, R., Qi, Y., Simon, G. P., and Estrin, Y., 2015, "Design of Responsive Materials Using Topologically Interlocked Elements," Smart Mater. Struct., **24**(2), p. 025034.
[35] Khandelwal, S., Cipra, R. J., Bolton, J. S., and Siegmund, T., 2015, "Adaptive Mechanical Properties of Topologically Interlocking Material Systems," Smart Mater. Struct., **24**(4), p. 045037.
[36] Carlesso, M., Molotnikov, A., Krause, T., Tushtev, K., Kroll, S., Rezwan, K., and Estrin, Y., 2012, "Enhancement of Sound Absorption Properties Using Topologically Interlocked Elements," Scr. Mater., **66**(7), pp. 483–486.
[37] Carlesso, M., Giacomelli, R., Krause, T., Molotnikov, A., Koch, D., Kroll, S., Tushtev, K., Estrin, Y., and Rezwan, K., 2013, "Improvement of Sound Absorption and Flexural Compliance of Porous Alumina-Mullite Ceramics by Engineering the Microstructure and Segmentation Into Topologically Interlocked Blocks," J. Eur. Ceram. Soc., **33**(13–14), pp. 2549–2558.
[38] Bréchet, Y. J. M., 2013, "Architectured Materials: An Alternative to Microstructure Control for Structural Materials Design? A Possible Playground for Bioinspiration?," *Materials Design Inspired by Nature*, Royal Society of Chemistry, Cambridge, UK, pp. 1–16.
[39] Mather, A., 2007, "Concepts in Improved Product Manufacturability and Reusability Through the Use of Topologically Interconnecting Structural Elements," Master's thesis, Purdue University, West Lafayette, IN.
[40] Brocato, M., Deleporte, W., Mondardini, L., and Tanguy, J.-E., 2014, "A Proposal for a New Type of Prefabricated Stone Wall," Int. J. Space Struct., **29**(2), pp. 97–112.
[41] Molotnikov, A., Estrin, Y., Dyskin, A. V., Pasternak, E., and Kanel-Belov, A. J., 2007, "Percolation Mechanism of Failure of a Planar Assembly of Interlocked Osteomorphic Elements," Eng. Fract. Mech., **74**(8), pp. 1222–1232.
[42] Golosovsky, M., Saado, Y., and Davidov, D., 1999, "Self-Assembly of Floating Magnetic Particles Into Ordered Structures: A Promising Route for the Fabrication of Tunable Photonic Band Gap Materials," Appl. Phys. Lett., **75**(26), pp. 4168–4170.
[43] Grzybowski, B. A., Stone, H. A., and Whitesides, G. M., 2000, "Dynamic Self-Assembly of Magnetized, Millimetre-Sized Objects Rotating at a Liquid–Air Interface," Nature, **405**(6790), pp. 1033–1036.
[44] Mirkhalaf, M., Tanguay, J., and Barthelat, F., 2016, "Carving 3D Architectures Within Glass: Exploring New Strategies to Transform the Mechanics and Performance of Materials," Extreme Mech. Lett., **7**, pp. 104–113.
[45] Mirkhalaf, M., and Barthelat, F., 2015, "A Laser-Engraved Glass Duplicating the Structure, Mechanics and Performance of Natural Nacre," Bioinspiration Biomimetics, **10**(2), p. 026005.
[46] Dugue, M., Fivel, M., Bréchet, Y., and Dendievel, R., 2013, "Indentation of Interlocked Assemblies: 3D Discrete Simulations and Experiments," Comput. Mater. Sci., **79**, pp. 591–598.
[47] Brugger, C., Fivel, M. C., and Bréchet, Y., 2009, "Numerical Simulations of Topologically Interlocked Materials Coupling DEM Methods and FEM Calculations: Comparison With Indentation Experiments," Symposium LL—Architectured Multifunctional Materials, MRS Proc., **1188**, p. LL05-05.
[48] Khandelwal, S., Siegmund, T., Cipra, R. J., and Bolton, J. S., 2014, "Scaling of the Elastic Behavior of Two-Dimensional Topologically Interlocked Materials Under Transverse Loading," ASME J. Appl. Mech., **81**(3), p. 031011.
[49] Brocato, M., and Mondardini, L., 2010, "Geometric Methods and Computational Mechanics for the Design of Stone Domes Based on Abeille's Bond," *Advances in Architectural Geometry 2010*, Springer-Verlag, Vienna, Austria, pp. 149–162.
[50] Khor, H. C., Dyskin, A. V., Estrin, Y., and Pasternak, E., 2004, "Mechanisms of Fracturing in Structures Built From Topologically Interlocked Blocks," International Conference on Structural Integrity and Fracture, SIF2004, Brisbane, Australia, Sept. 26–29, Australian Fracture Group, Inc., Perth, Australia, pp. 189–194.
[51] Block, P., and Ochsendorf, J., 2007, "Thrust Network Analysis: A New Methodology for Three-Dimensional Equilibrium," J. Int. Assoc. Shell Spat. Struct., **48**(3), pp. 167–173.
[52] Block, P., and Lachauer, L., 2014, "Three-Dimensional Funicular Analysis of Masonry Vaults," Mech. Res. Commun., **56**, pp. 53–60.
[53] Siegmund, T., Khandelwal, S., Wheatley, B., Varanasi, S., Cipra, R., and Bolton, S., 2013, "Multifunctional Composites by Segmentation and Assembly," International Conference on Composite Materials (ICCM-19), Montreal, QC, Canada, July 28–Aug. 2, pp. 23–31.
[54] Calladine, C. R., 1978, "Buckminster Fuller's 'Tensegrity' Structures and Clerk Maxwell's Rules for the Construction of Stiff Frames," Int. J. Solids Struct., **14**(2), pp. 161–172.
[55] Bowden, L., Byrne, H., Maini, P., and Moulton, D., 2015, "A Morphoelastic Model for Dermal Wound Closure," Biomech. Model. Mechanobiol., **15**(3), pp. 663–681.

[56] Konrad, W., Flues, F., Schmich, F., Speck, T., and Speck, O., 2013, "An Analytic Model of the Self-Sealing Mechanism of the Succulent Plant Delosperma Cooperi," J. Theor. Biol., **336**, pp. 96–109.
[57] Busch, S., Seidel, R., Speck, O., and Speck, T., 2010, "Morphological Aspects of Self-Repair of Lesions Caused by Internal Growth Stresses in Stems of Aristolochia Macrophylla and Aristolochia Ringens," Proc. R. Soc. London, Ser. B, **277**(1691), pp. 2113–2120.
[58] Lambert, J., and Jonas, G., 1976, "Towards Standardization in Terminal Ballistics Testing: Velocity Representation," USA Ballistic Research Laboratories, Aberdeen Proving Ground, MD, Technical Report No. 1852.
[59] Wardiningsih, W., Troynikov, O., Molotnikov, A., and Estrin, Y., 2013, "Influence of Protective Pad Integrated Into Sport Compression Garments on Their Pressure Delivery to Athlete's Lower Limbs," Procedia Eng., **60**, pp. 170–175.
[60] Estrin, Y., Dyskin, A. V., Pasternak, E., Khor, H. C., and Kanel-Belov, A. J., 2010, "Topological Interlocking of Protective Tiles for the Space Shuttle," Philos. Mag. Lett., **83**(6), pp. 351–355.
[61] Dyskin, A. V., Estrin, Y., Pasternak, E., Khor, H. C., and Kanel-Belov, A. J., 2005, "The Principle of Topological Interlocking in Extraterrestrial Construction," Acta Astronaut., **57**(1), pp. 10–21.
[62] Barthelat, F., 2015, "Architectured Materials in Engineering and Biology: Fabrication, Structure, Mechanics and Performance," Int. Mater. Rev., **60**(8), pp. 413–430.
[63] Fratzl, P., Kolednik, O., Fischer, F. D., and Dean, M. N., 2016, "The Mechanics of Tessellations—Bioinspired Strategies for Fracture Resistance," Chem. Soc. Rev., **45**(2), pp. 252–267.
[64] Barthelat, F., Yin, Z., and Buehler, M. J., 2016, "Structure and Mechanics of Interfaces in Biological Materials," Nat. Rev. Mater., **1**(4), p. 16007.